J Mater Sci: Mater Electron (2016) 27:3619–3627
DOI 10.1007/s10854-015-4199-1

Simple synthesis and characterization of nickel phosphide nanostructures assisted by different inorganic precursors

Azam Sobhani[1] · **Masoud Salavati-Niasari**[2]

Received: 18 November 2015 / Accepted: 8 December 2015 / Published online: 14 December 2015

Abstract Nickel phosphide nanostructures were prepared by thermal decomposition method from different inorganic precursors, such as: bis(salicylidene)nickel(II) [$Ni(sal)_2$], bis(salicylate)nickel(II) [$Ni(Hsal)_2$], nickel oxalate [$Ni(O_4C_2)(H_2O)_4$] and nickel-*o*-phthalate [$Ni(pht)(H_2O)_2$]. Nickel(II) acetate tetrahydrate $Ni(CH_3COO)_2{\cdot}4H_2O$ was used as reference. Nanostructural control of products prepared through the thermolysis of precursors using triphenylphosphine as a surfactant solvent and phosphorus precursor was reported. The SEM and TEM images show the morphology and particle size of the as-synthesized nanostructures. The XRD patterns show mixed-phase hexagonal Ni_2P/tetragonal $Ni_{12}P_5$ (represented as Ni_xP_y). The FT-IR spectroscopy confirms that the products prepared are Ni_xP_y phase, which is in agreement with XRD results.

1 Introduction

In recent years, extensive attention has been paid to the nanomaterials owing to their interesting properties and potential applications [1–10]. Hence, investigations on the synthesis and modification of nanosized phosphids have attracted tremendous attentions. Transition metal phosphides are important materials with a wide variety of useful properties, including superconductivity [11, 12], magnetic behavior [13], magnetoresistance [14] and Li intercalation capacity for battery applications [15]. They are a novel catalyst group for deep hydrotreating and have received much attention due to their high activity for hydrodesulfurization (HDS) and hydrodenitrogenation (HDN) of petroleum feedstocks [14]. Ni_2P is an n-type semiconductor with a bulk band gap of 1.0 eV with potential uses in solar cells and catalysis [16]. The solid-state Ni_2P is well-known as a corrosion-resistant and oxidation-resistant material [17]. In contrast to sulfides which adopt planar morphologies, phosphides are not layered compounds and form spherical particles which can be well dispersed on supports.

Researchers have utilized several methods to synthesize nickel phosphide nanostructures, such as: solvothermal [18], phosphate reduction [19], thermal decomposition [20], direct combination of the elements, organic solution-phase technique [21], surface-phosphatizing Ni nanoparticles [17] and ball milling route [22]. In this study we focused on preparing Ni_xP_y nanostructures through thermal decomposition process using TPP ($C_{18}H_{15}P$) as phosphorus source and oleylamine ($C_{18}H_{37}N$) as surfactant. By controlling the growth of the particles, surfactants play an important role in synthetic procedure and lead to products with controlled size and a narrow size distribution. In addition of the important role of surfactants in size control of the products, precursors with special shapes also can prevent from agglomeration [23]. This method is based on the ability of the TPP molecule to act as P atom donors, through thermal decomposition at temperatures above 300 °C. Trioctylphosphine oxide (TOPO), TOP [24, 25], TPP [26], tris(trimethylsilyl) phosphine [27] and white

✉ Azam Sobhani
sobhaniazam@gmail.com

✉ Masoud Salavati-Niasari
salavati@kashanu.ac.ir

[1] Department of Chemistry, Kosar University of Bojnord, Bojnord, Islamic Republic of Iran

[2] Institute of Nano Science and Nano Technology, University of Kashan, P. O. Box 87317–51167, Kashan, Islamic Republic of Iran

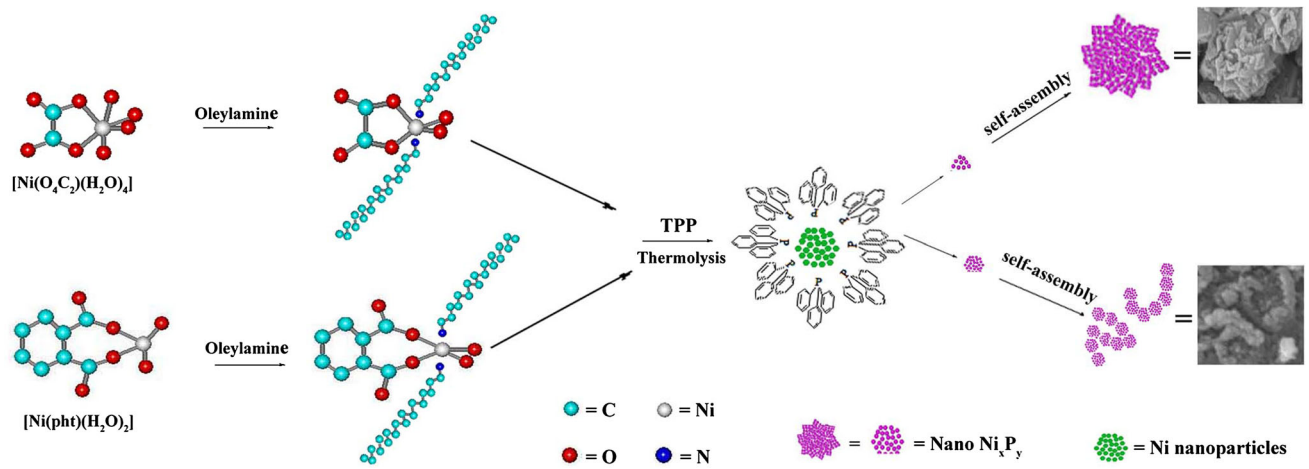

Scheme 1 Schematic diagram illustrating the formation of Ni_xP_y nanostructures

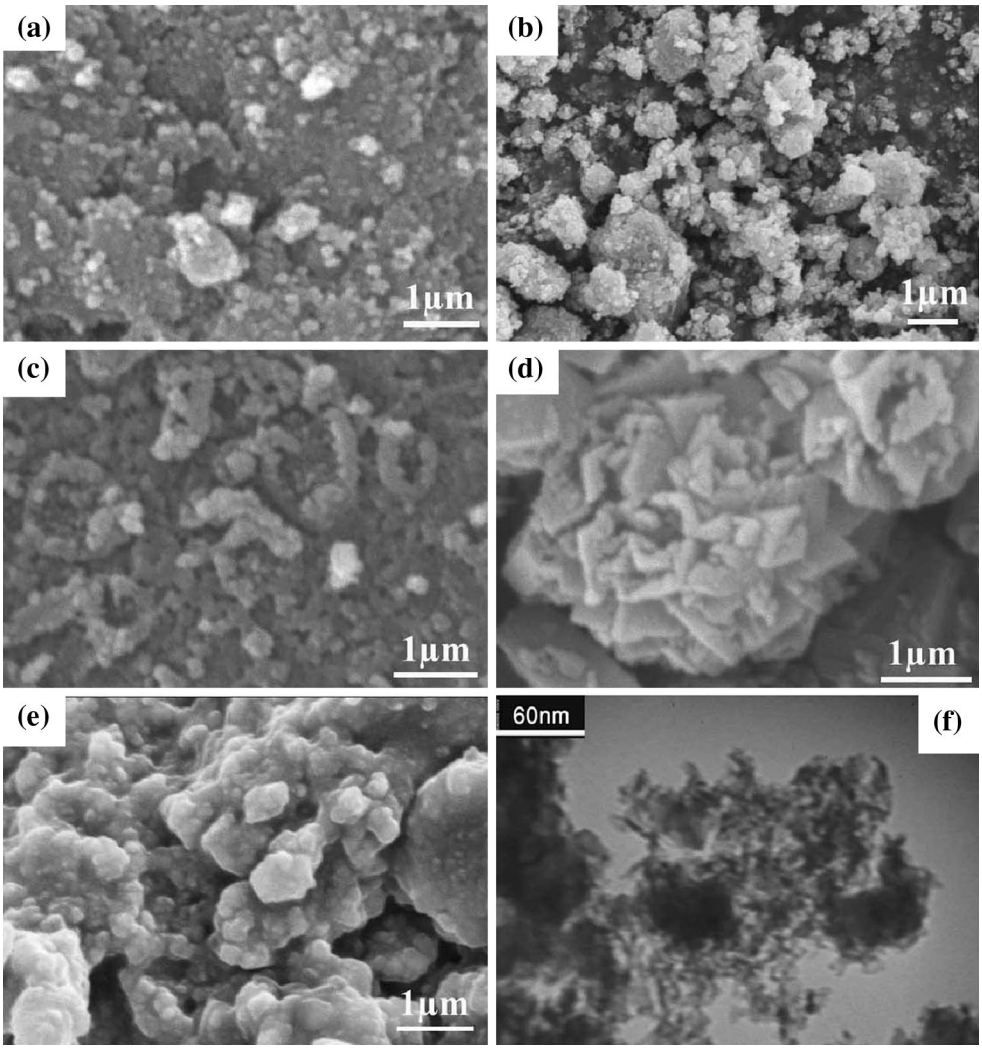

Fig. 1 SEM images of Ni_xP_y nanostructures prepared from **a** $[Ni(sal)_2]$, **b** $[Ni(Hsal)_2]$, **c** $[Ni(pht)(H_2O)_2]$, **d** $[Ni(O_4C_2)(H_2O)_4]$, **e** $Ni(CH_3COO)_2{\cdot}4H_2O$ and **f** TEM image of sample obtained from $[Ni(sal)_2]$

phosphorus [28] have been introduced as phosphorus reagents for the synthesis of metal phosphides. Several studies of metal phosphide formation suggesting that metals can cause cleavage of the P–C bond, resulting in diffusion of phosphorus into the metal.

In this article, the effect of the Ni precursors in the formation and characterization of Ni_xP_y nanostructures are considered. To study this effect, four types of precursor powders were used: $[Ni(sal)_2]$, $[Ni(Hsal)_2]$, $[Ni(O_4C_2)(H_2O)_4]$ and $[Ni(pht)(H_2O)_2]$. In all cases, there is a remarkable correlation between type of the metal precursors and structure, size and morphology of metal phosphide products. The concept of co-assembling inorganic precursor molecules with amphiphile organic molecules for controlling the structure and organization of inorganic materials has successfully been used to produce materials with both scientific and technological importance. At the moment a major interest is in the development of organometallic or inorganic precursors.

2 Experimental

2.1 Materials and experiments

The precursor complexes were prepared according to the procedures described previously and were characterized by FT-IR, elemental analyses and thermogravimetric analysis (TGA) [29–33]. Oleylamine, TPP, toluene, hexane, and ethanol were purchased from Aldrich and used as received. The XRD patterns were collected from a diffractometer of Philips company with X'PertPro monochromatized Cu Ka radiation (k = 1.54 Å). Microscopic morphology of products was visualized by a LEO 1455VP scanning electron microscope (SEM). GC-2550TG (Teif Gostar Faraz Company, Iran) were used for all chemical analyses. Transmission electron microscopy (TEM) image was obtained on a Philips EM208 transmission electron microscope with an accelerating voltage of 200 kV. Fourier transform infrared (FT-IR) spectra were recorded on Shimadzu Varian 4300 spectrophotometer in KBr pellets.

2.2 Synthesis of Ni_xP_y nanostructures

The overall synthetic procedure is shown in Scheme 1. This synthetic procedure is a modified version of the method developed by Hyeon et al. [34]. In this synthesis, a certain amount of nickel precursor and oleylamine loaded in a 50 ml three-neck distillation were heated up to 120 °C for 60 min. Green solution was generated with the gradual dissolution of precursor complex. Then, TPP was dissolved in the mixture. The solution was aged at 300 °C for 30 min. The color of the reaction mixture changes from green to dark green and finally black. The thermal decomposition of the precursor complexes at 300 °C led to a formation of Ni_xP_y nanostructures. The nanostructures were precipitated by adding excess ethanol to the solution. The precipitate was collected via centrifugation after

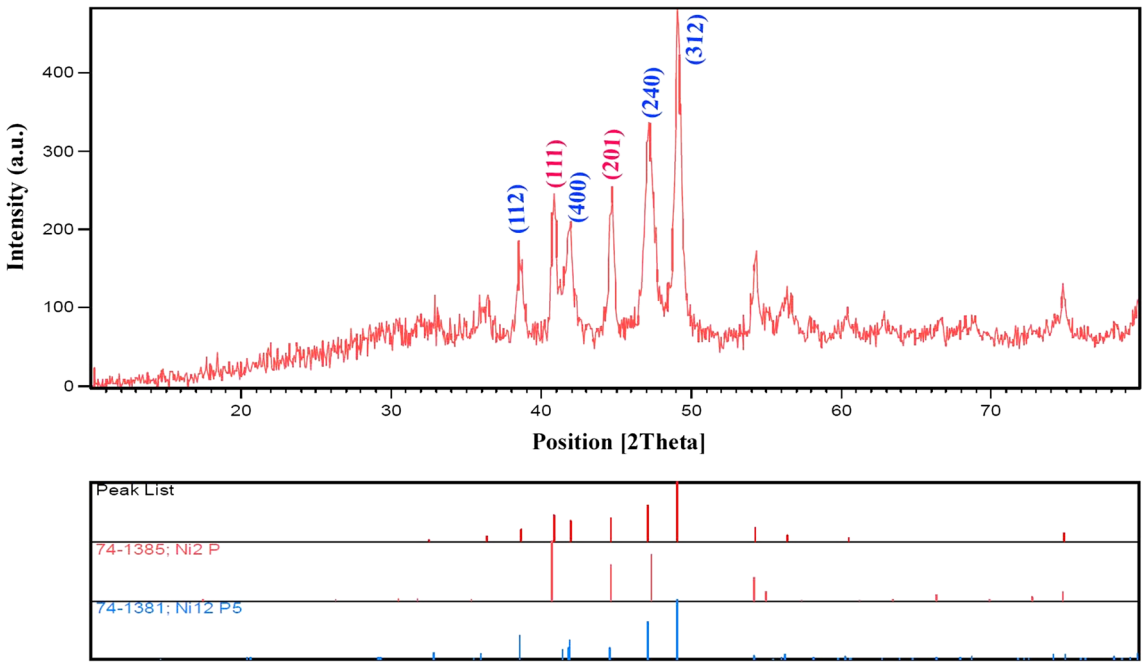

Fig. 2 XRD pattern of Ni_xP_y nanostructures obtained from $[Ni(sal)_2]$

Table 1 XRD results of Ni_xP_y nanostructures obtained from the $[Ni(sal)_2]$ precursor

Reference code (JCPDS)	Chemical formula	Planes (hkl)	Crystal system	Space group	Unit cell parameters (nm)		
					a	b	c
74-1385	Ni_2P	(111) (201)	Hexagonal	P-62 m	0.5859	0.5859	0.3382
74-1381	$Ni_{12}P_5$	(312) (240) (400) (112)	Tetragonal	I4/m	0.8646	0.8646	0.5070

15 min of stirring and could easily be re-dispersed in nonpolar organic solvents, such as hexane or toluene. Some control experiments, in which nickel precursors were replaced by manganese and cadmium precursors and other operational processes were unchanged, were performed.

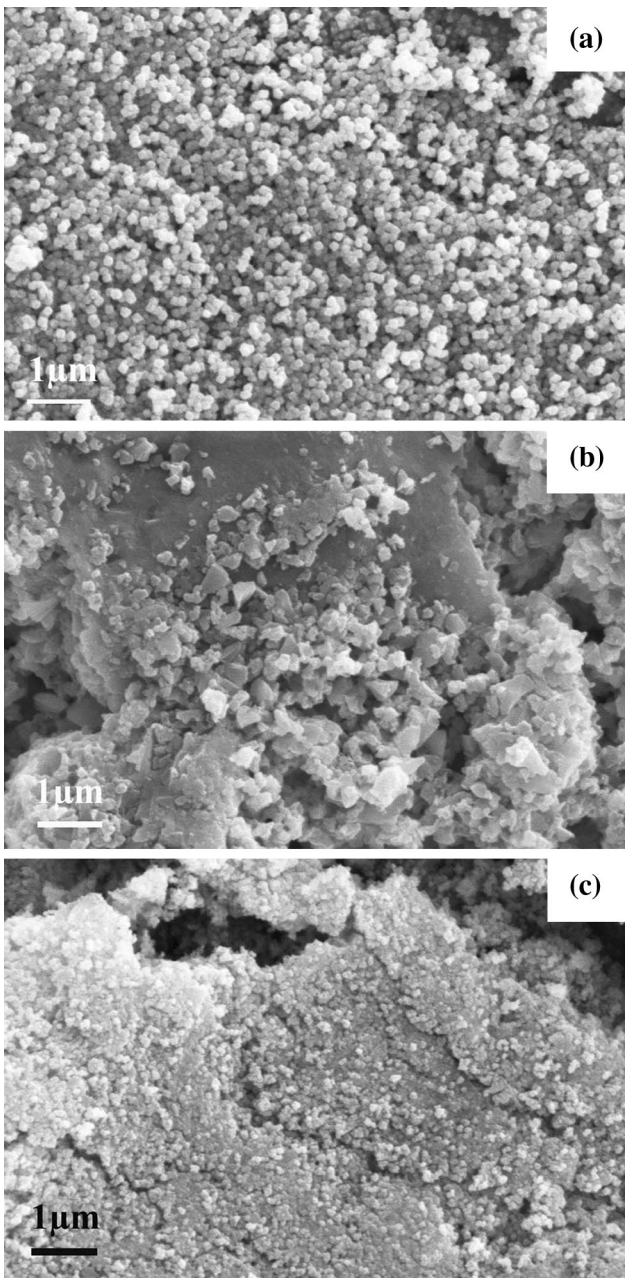

Fig. 3 SEM images of nanostructures prepared from **a** $[Mn(sal)_2]$, **b** $[Mn(O_4C_2)(H_2O)_2]$ and **c** $Mn(CH_3COO)_2{\cdot}4H_2O$

3 Results and discussion

Since many fundamental properties of semiconductor materials have been expressed as a function of the size and the shape, the control of nucleation and growth of nanostructural materials is becoming critical [35]. The use of different nickel precursors leads to the formation of nickel phosphide species with different shapes and sizes that having different characteristics. During thermal decomposition reaction, nucleation rate for nanostructures can reach a high value in a short time and these nuclei are wrapped by surfactant. Consequently, the formed nanostructures grow to a certain value and saturate. The effect of the surfactant is to control the size of the crystals and to prevent the aggregation of crystals. When the concentration of the surfactant is low, the nuclei can not be wrapped by the surfactant completely and wide size distribution of nanostructures is obtained. The oleylamine is known as a ligand that binds tightly to the nanostructures surface. The TPP is a high-boiling point surfactant with a patulous long-chain structure providing greater steric hindrance, also act as a phosphorus precursor.

The morphology of the nickel phosphides obtained from different precursors is investigated by SEM, as shown in Fig. 1. The products obtained from $[Ni(sal)_2]$, $[Ni(Hsal)_2]$ and $[Ni(pht)(H_2O)_2]$ are agglomerated nanoparticles. These nanoparticles are spherical in shape and smooth on their surfaces. It can be observed that with the change of precursor of $[Ni(sal)_2]$ to $[Ni(pht)(H_2O)_2]$ and then to $[Ni(Hsal)_2]$, the particle size and agglomeration of the nanoparticles increase. The products obtained from $[Ni(O_4C_2)(H_2O)_4]$ are flower-like in shape with uneven surfaces. Adding benzene ring to nickel oxalate to produce nickel-*o*-phthalate, influences size and morphology of products. In $[Ni(pht)(H_2O)_2]$, co-assembling inorganic molecules with organic molecules produces nanoparticles with uniform size distribution that have average diameter 100 nm. These nanoparticles are agglomerated and U-shaped structures produced. $[Ni(O_4C_2)(H_2O)_4]$ precursor in the ratio of $[Ni(pht)(H_2O)_2]$ precursor has smaller size, lower steric hindrance and larger surface to volume ratios,

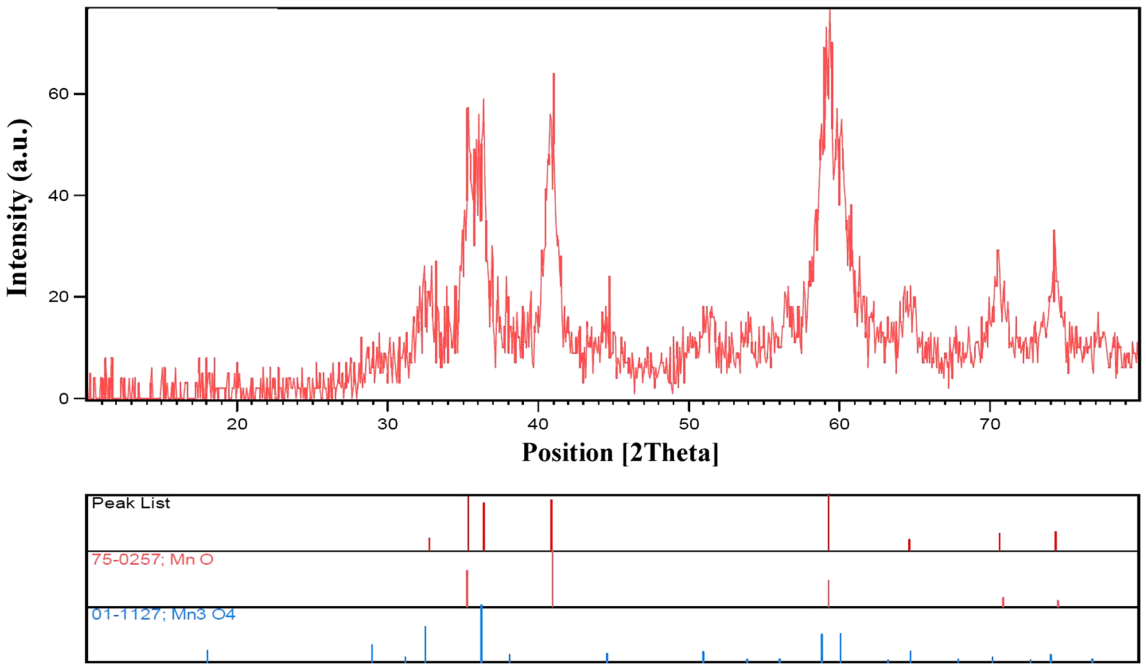

Fig. 4 XRD pattern of nanostructures obtained from $[Mn(sal)_2]$

consequently possible of aggregation of precursor molecules is more. Therefore products obtained from this precursor (parallelepipeds) are collected and formed flowers which can be clearly seen in the Fig. 1d. These flowers are in micrometer size. Figure 1e shows the SEM image of sample obtained from nickel acetate. This figure shows the particles coalesce and turn into bulk structures, when use from nickel acetate as precursor. In order to further elucidate the size and the crystal structure of the products, TEM image was taken. TEM image of sample obtained from $[Ni(sal)_2]$ has been shown in Fig. 1f. The image shows the products obtained from $[Ni(sal)_2]$ are very small nanoparticles with a diameter less of 10 nm.

The XRD pattern of the Ni_xP_y nanostructures obtained from the $[Ni(sal)_2]$, is depicted in Fig. 2. It can be seen that the products have the peaks corresponding to hexagonal Ni_2P and tetragonal $Ni_{12}P_5$ phases. The XRD results have been summarized in Table 1. In comparison with other reports of pure [36] and less-pure [37] Ni_2P phases, $Ni_{12}P_5$ might form under milder conditions, whereas the conversion to pure Ni_2P could require prolonged growth times or higher temperatures than those reported here [38, 39]. In Fig. 2, the peaks corresponding to Ni_2P and $Ni_{12}P_5$ are indicated with red and blue colors, respectively. The intense and sharp diffraction peaks suggest that the obtained product is well crystallized.

For investigating the effect of precursor on the morphology and particle size of the products, manganese and cadmium complexes were also used as precursors. Figure 3 shows SEM images of nanostructures prepared from different manganese precursors. The images show granular morphology. There is a great deal of spherical nanoparticles in this figure. It can be observed that with the change of precursor of $Mn(CH_3COO)_2{\cdot}4H_2O$ to $[Mn(sal)_2]$ and then $[Mn(O_4C_2)(H_2O)_2]$, morphology of samples remains nearly constant and only particle size and agglomeration of nanoparticles increase.

According to the XRD pattern of samples obtained from manganese precursors (Fig. 4), the peaks are broad and ambiguous, that show the lower yield of products. Two types of manganese oxides, MnO and Mn_3O_4, can be found in the resulting products. As shown in this figure, the expected products could not be obtained (manganese phosphides) in this conditions.

Figure 5 shows the SEM images of samples obtained from six different cadmium precursors including $[Cd(sal)_2(H_2O)_2]$, $[Cd(Hsal)_2(H_2O)_2]_2$, $[Cd(pht)(H_2O)]_n$, $[Cd(C_2O_4)(H_2O)]$, cadmium catechol and $Cd(CH_3COO)_2{\cdot}2H_2O$. The formation of regular geometric structures with different sizes clearly observes in Fig. 5a, f. These octahedral structures are obtained from $[Cd(sal)_2(H_2O)_2]$ and cadmium acetate. When use from $[Cd(Hsal)_2(H_2O)_2]_2$ precursor, semi-spherical planes are formed (Fig. 5b). The samples obtained from phthalate and catechol precursors are spherical nanoparticles (Fig. 5c, e, respectively). The nanoparticles obtained from cadmium catechol are agglomerated. The irregular geometric structures with different sizes are products obtained from cadmium oxalate (Fig. 5d).

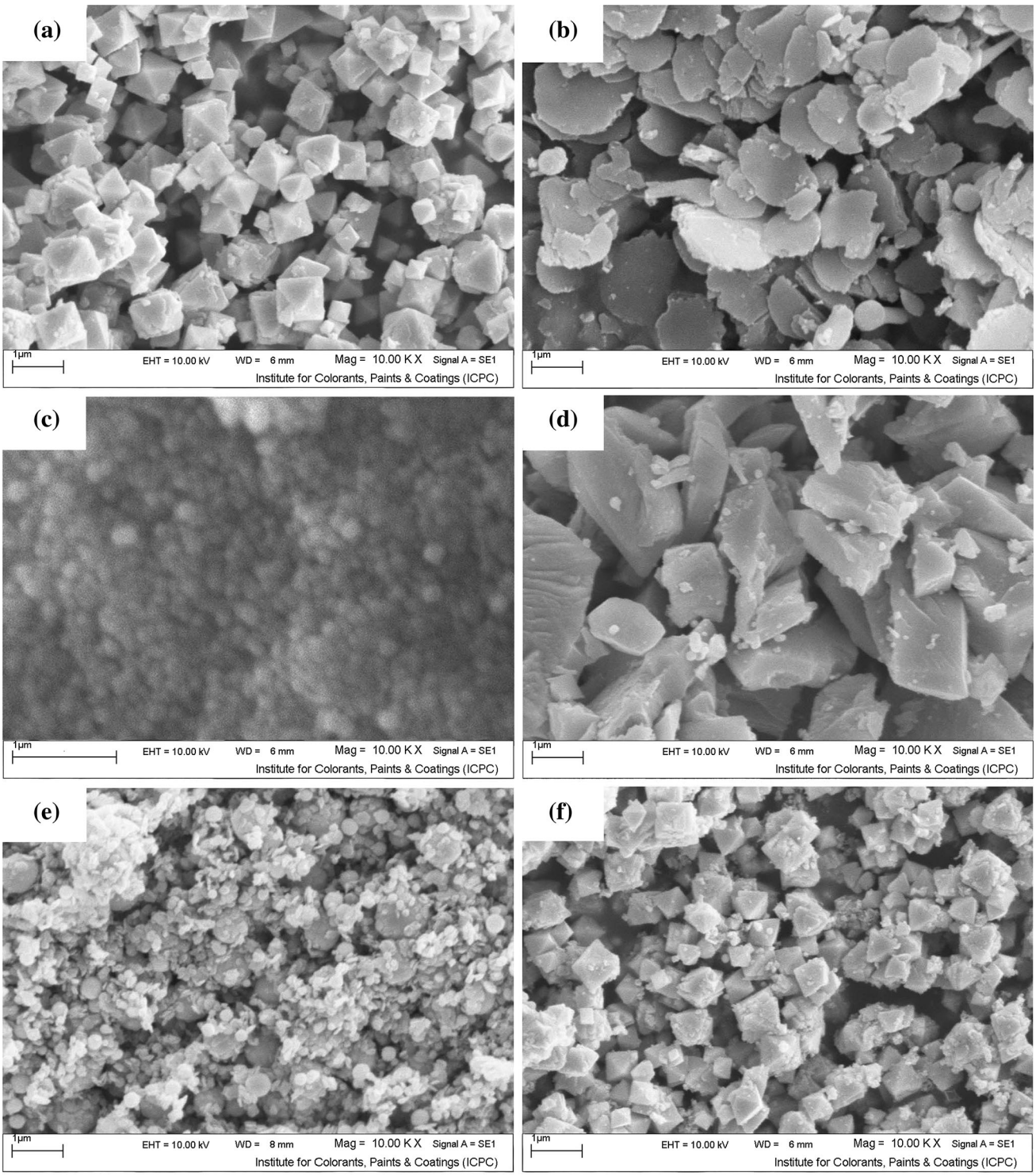

Fig. 5 SEM images of nanostructures prepared from (a) $[Cd(sal)_2(H_2O)_2]$, (b) $[Cd(Hsal)_2(H_2O)_2]_2$, (c) $[Cd(pht)(H_2O)]_n$, (d) $[Cd(C_2O_4)(H_2O)]$, (e) cadmium catechol and (f) $Cd(CH_3COO)_2.2H_2O$

Figure 6 shows XRD patterns of nanostructures obtained from three different cadmium precursors. The products are found to be the cubic CdO. As a result, the expected products (cadmium phosphids) could not be obtained from cadmium precursors and the products are not ideal.

Figure 7 shows FT-IR spectra of (a) *o*-phthalic acid with point group C_2 [40] (b) $[Ni(pht)(H_2O)_2]$ obtained at 100 °C

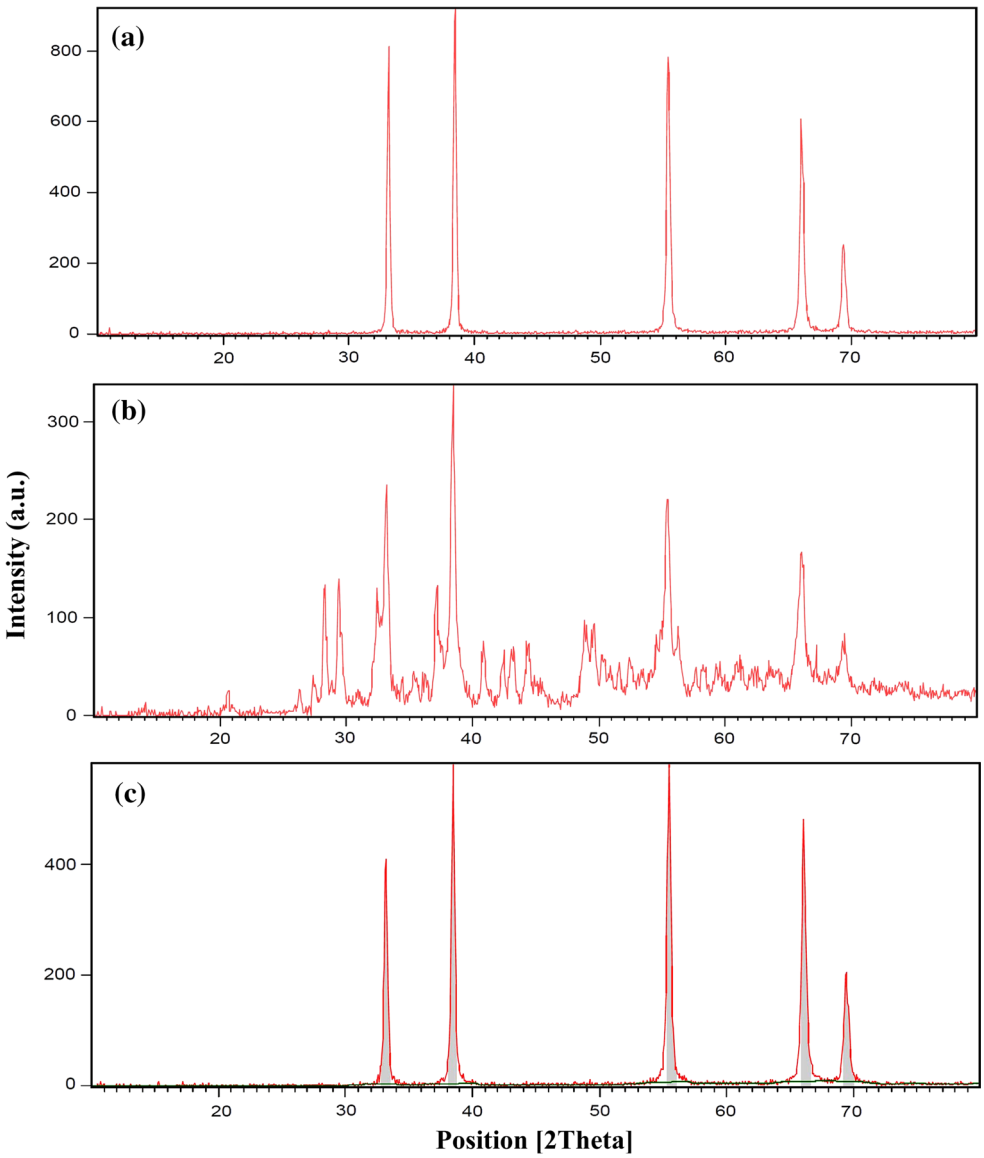

Fig. 6 XRD patterns of nanostructures obtained from: **a** $[Cd(sal)_2(H_2O)_2]$, **b** $[Cd(Hsal)_2(H_2O)_2]_2$ and **c** $[Cd(pht)(H_2O)]_n$

(c) oleylamine and (d) Ni_xP_y nanostructures obtained from the $[Ni(pht)(H_2O)_2]$ precursor. Figure 7b has no broad absorption bands at 3260–3200 cm^{-1} and a sharp band at 1630–1600 cm^{-1}. Therefore, there are not crystallization water molecules in the outer sphere [41]. In this spectrum the broad absorption band centered at 3423 cm^{-1} is attributable to the ν(OH) stretching vibrations which indicates the presence of physisorbed and coordinated water linked to precursor [42]. The C=O band at 1698 cm^{-1} in the FT-IR spectrum of the *o*-phthalic acid does not appear in the precursor one which indicates the absence of uncoordinated ophthalmic acid in precursor. Two very strong peaks at 1556 and 1414 cm^{-1} can be attributed to the asymmetric and symmetric stretching vibrations of coordinated carboxylate groups. The separation between the asymmetric and symmetric stretching frequencies ($\Delta\nu = \nu_{asym} - \nu_{sym}$) is 142 cm^{-1} which indicates the *o*-phthalic acid ligand is bidentate coordinating through both carboxylic groups [43]. The weak peaks at 1486 and 1359 cm^{-1} correspond to ν(CC) and medium peaks at 734 and 695 cm^{-1} is assigned to γ(CH) and the weak peak at 1143 cm^{-1} is attributable to δ(CH) of benzene ring and all of remaining weak peaks are due to benzene ring vibrations. The FT-IR spectrum of free oleylamine and Ni_xP_y nanostructures are shown in Fig. 7c, d, respectively. The oleylamine is known as a ligand that binds tightly to the nanostructures surface. In Fig. 7d two weak peak at 2919 and 2850 cm^{-1} attributing to the C–H stretching models of the oleylamine carbon chain. The only difference among these characteristic peaks is either the peak intensity or a slight shift in the peak position that indicating oleylamine molecules have been absorbed on the surface of Ni_xP_y

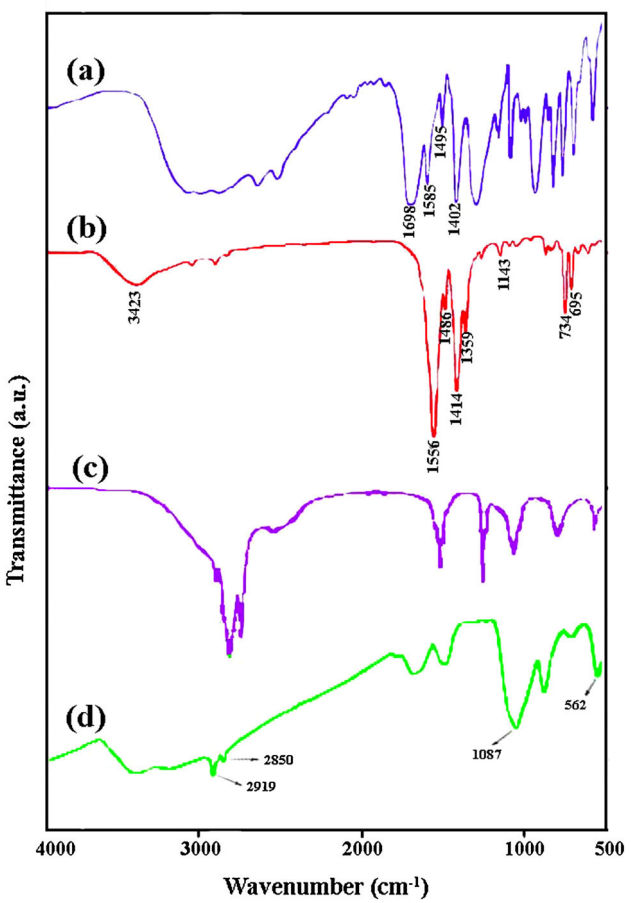

Fig. 7 FT-IR spectra of (*a*) *o*-phthalic acid, (*b*) $[Ni(pht)(H_2O)_2]$, (*c*) oleylamine and (*d*) Ni_xP_y nanostructures obtained from the $[Ni(pht)(H_2O)_2]$

nanostructures. Because the precipitates are washed with ethanol several times and all the residual surfactant is removed, the characteristic peaks of the oleylamine and TPP are introduced from the oleylamine and TPP coated surface of Ni_xP_y nanoparticles [44]. Two peaks at 3413 and 1625 cm^{-1}, in curve 7d, are assigned to the stretching and bending vibration of absorption water on surface of nano Ni_xP_y, respectively. The peak around 562 and 725 cm^{-1} shows a distinct stretching mode of Ni_xP_y nanostructures. This pattern further confirmed that the products prepared from thermal decomposition are Ni_xP_y phase, which is in agreement with analysis result of XRD. This spectrum has no characteristic peaks of impurities or other precursor compounds.

4 Conclusions

In summary, Ni_xP_y nanostructures have been prepared by a thermal decomposition process in a binary surfactant solvent of TPP and oleylamine using four different types of precursors. The use of different precursors and preparation routes play an important role on the properties of nanostructures. The following sequence of particle size of Ni_xP_y nanostructures is pointed out: $Ni_xP_{y\,[Ni(sal)_2]} < Ni_xP_{y\,[Ni(pht)(H_2O)_2]} < Ni_xP_{y\,[Ni(Hsal)_2]} < Ni_xP_{y\,[Ni(O_4C_2)(H_2O)_4]}$. This reaction route is simple and can further be applied to prepare other metal phosphides.

Acknowledgments Authors are grateful to the council of University of Kashan for supporting this work by Grant No (159271/452).

References

1. A. Sobhani, M. Salavati-Niasari, Synthesis and characterization of a nickel selenide series via a hydrothermal process. Superlattices Microstruct. **65**, 79 (2014)
2. A. Sobhani, M. Salavati-Niasari, Synthesis and characterization of CdSe nanosturctures by using a new selenium source: effect of hydrothermal preparation conditions. Mater. Res. Bull. **53**, 7 (2014)
3. A. Sobhani, M. Salavati-Niasari, A new simple route for the preparation of nanosized copper selenides under different conditions. Ceram. Int. **40**, 8173 (2014)
4. A. Sobhani, M. Salavati-Niasari, Hydrothermal synthesis, characterization, and magnetic properties of cubic $MnSe_2$/Se nanocomposites material. J. Alloys Compd. **617**, 93 (2014)
5. A. Sobhani, M. Salavati-Niasari, A polyethylene glycol-assisted hydrothermal synthesis of $FeSe_2$ nanoparticles and $FeSe_2$/FeO(OH) Nanocomposites. J. Alloys Compd. **625**, 26 (2015)
6. F. Ansari, A. Sobhani, M. Salavati-Niasari, Sol-gel auto-combustion synthesis of $PbFe_{12}O_{19}$ using maltose as a novel reductant. RSC Adv. **4**, 63946 (2014)
7. A. Sobhani, M. Salavati-Niasari, CdSe nanoparticles: facile hydrothermal synthesis, characterization and optical properties. J. Mater. Sci. Mater. Electron. **26**, 6831 (2015)
8. M. Masjedi-Arani, M. Salavati-Niasari, A simple sonochemical approach for synthesis and characterization of Zn_2SiO_4 nanostructures. Ultrason. Sonochem. **29**, 226 (2016)
9. M. Masjedi, N. Mir, E. Noori, T. Gholami, M. Salavati-Niasari, Effect of Schiff base ligand on the size and the optical properties of TiO_2 nanoparticles. Superlattices Microstruct. **62**, 30 (2013)
10. M. Masjedi-Arani, M. Salavati-Niasari, D. Ghanbari, G. Nabiyouni, A sonochemical-assisted synthesis of spherical silica nanostructures by using a new capping agent. Ceram. Int. **40**, 495 (2014)
11. J. Jiang, S.M. Kauzlarich, Chem. Mater. **18**, 435 (2006)
12. D.C.S. Souza, V. Pralong, A.J. Jacobson, L.F. Nazar, Science **296**, 2012 (2002)
13. M.-P. Bichat, J.-L. Pascal, F. Gillot, F. Favier, Chem. Mater. **17**, 6761 (2005)
14. S.T. Oyama, J. Catal. **216**, 343 (2003)
15. A. Panneerselvam, M.A. Malik, M. Afzaal, P. O'Brien, M. Helliwellt, J. Am. Chem. Soc. **130**, 2420 (2008)
16. M. Sharon, G. Tamizhmani, J. Mater. Sci. **21**, 2193 (1986)
17. X. Zheng, S. Yuan, Z. Tian, S. Yin, J. He, K. Liu, L. Liu, Chem. Mater. **21**, 4839 (2009)
18. J. Liu, X. Chen, M. Shao, C. An, C. Yu, Y. Qian, J. Cryst. Growth **252**, 297 (2003)
19. S. Yang, C. Liang, R. Prins, J. Catal. **241**, 465 (2006)
20. J. Park, B. Koo, K.Y. Yoon, Y. Hwang, M. Kang, J.G. Park, T. Hyeon, J. Am. Chem. Soc. **127**, 8433 (2005)
21. R.K. Chiang, R.T. Chiang, Inorg. Chem. **46**, 369 (2007)

22. S. Boyanov, K. Annou, C. Villevieille, M. Pelosi, D. Zitoun, L. Monconduit, Nanostructured transition metal phosphide as negative electrode for lithium-ion batteries. Ionics **14**, 183 (2008)
23. M. Salavati-Niasari, N. Mir, F. Davar, Inorg. Chim. Acta **363**, 1719 (2010)
24. A.E. Henkes, Y. Vasquez, R.E. Schaak, J. Am. Chem. Soc. **129**, 1896 (2007)
25. R.K. Chiang, R.T. Chiang, Inorg. Chem. **46**, 369 (2007)
26. X. Zheng, S. Yuan, Z. Tian, S. Yin, J. He, K. Liu, L. Liu, Chem. Mater. **21**, 4839 (2009)
27. S.C. Perera, G. Tsoi, L.E. Wenger, S.L. Brock, J. Am. Chem. Soc. **125**, 13960 (2003)
28. S. Carenco, I. Resa, X. Le Goff, P. Le Floch, N. Mézailles, Chem. Commun. 2568 (2008)
29. M. Salavati-Niasari, N. Mir, F. Davar, Polyhedron **28**, 1111 (2009)
30. M. Salavati-Niasari, F. Mohandes, F. Davar, M. Mazaheri, M. Monemzadeh, N. Yavarinia, Inorg. Chim. Acta **362**, 3691 (2009)
31. M. Salavati-Niasari, M. Shaterian, M.R. Ganjalim, P. Norouzi, J. Mol. Catal. A Chem. **261**, 147 (2007)
32. P. Kokkonen, L.H.J. Lajunen, L. Palmu, Therm. Acta **114**, 145 (1987)
33. L. Li, L. Yuan, Y. Yang, K. Zhang, J. Sun, Guang Pu Xue Yu Guang Pu Fen Xi **20**, 671 (2000)
34. J. Park, E. Kang, S.U. Son, H.M. Park, M.K. Lee, J. Kim, K.W. Kim, H.J. Noh, J.H. Park, C.J. Bae, J.G. Park, T. Hyeon, Adv. Mater. **17**, 429 (2005)
35. J. Yang, J.H. Zeng, S.H. Yu, L. Yang, G.E. Zhou, Y.T. Qian, Chem. Mater. **12**, 3259 (2000)
36. A.E. Henkes, Y. Vasquez, R.E. Schaak, J. Am. Chem. Soc. **129**, 1896 (2007)
37. R.K. Chiang, R.T. Chiang, Inorg. Chem. **46**, 369 (2007)
38. A.E. Henkes, R.E. Schaak, Chem. Mater. **19**, 4234 (2007)
39. K. Senevirathne, A.W. Burns, M.E. Bussell, S.L. Brock, Adv. Funct. Mater. **17**, 3933 (2007)
40. G.M. Duffy, S.C. Pillai, D.E. Mccormack, Smart Mater. Struct. **16**, 1379 (2007)
41. W. Brzyska, D. Wańczowska-Fonfara, J. Therm. Anal. **35**, 727 (1989)
42. J.F. Arenas, J.I. Marcos, Spectrochim. Acta A. **36**, 1075 (1980)
43. W. Brzyska, W. Wolodkiewicz, J. Therm. Anal. **34**, 1207 (1988)
44. M. Salavati-Niasari, F. Davar, M. Mazaheri, M. Shaterian, J. Magn. Magn. Mater. **320**, 575 (2008)